Solar-Terrestrial Physics. 2025, vol. 11, iss. 3, pp. 91–97. DOI: 10.12737/stp-113202511. © 2025 A.A. Karakhanyan, S.I. Molodykh. Published by INFRA-M Academic Publishing House

DOI: 10.12737/stp-113202511

Received March 18, 2025
Accepted July 08, 2025

METEOROLOGICAL RESPONSE TO CHANGES IN IONOSPHERIC ELECTRIC POTENTIAL CAUSED BY DISTURBED SOLAR WIND

A.A. Karakhanyan
Institute of Solar-Terrestrial Physics SB RAS, Irkutsk, Russia, asha@iszf.irk.ru

S.I. Molodykh
Institute of Solar-Terrestrial Physics SB RAS, Irkutsk, Russia, sim@iszf.irk.ru

Abstract. The ionospheric electric potential (EP) is utilized as a characteristic of the solar forcing to determine the tropospheric response during strong disturbances. We compare EP calculations carried out using the 2001 and 2005 versions of the Weimer model. Differences in the spatial distribution of EP during geomagnetic superstorms have been revealed for the models considered. The behavior of EP anomalies and contrast averaged over high latitudes is shown. The EP contrast is the difference between EP anomalies averaged over regions of the same sign. It has been found that changes in EP anomalies differ in different versions of the model, whereas EP contrast variations, calculated by both versions, behave synchronously during disturbances. Correlation analysis of variations in the averaged EP contrast with variations in the *PC* geomagnetic index has shown that both can be used as indicators of solar activity to study individual geomagnetic superstorms. An increase in the EP contrast is accompanied by an increase in the contrast of the meteorological parameters, in particular in the contrast of high clouds during disturbances.

Keywords: ionospheric electric potential, geomagnetic superstorm, geomagnetic index, outgoing longwave radiation, cloud, water vapor, climate.

INTRODUCTION

The second wave of climate warming over the instrumental observation period, which began in the 1970s and intensified in the 1990s, is currently manifested as a sharp increase in the number of dangerous phenomena on the planet [Mokhov, 2023; https://www.ipcc.ch/report/ar6/syr/]. One of the possible causes of the climate changes is the effect of solar activity on Earth's atmosphere. The absence of a direct mechanism of the effect of solar activity on the lower atmosphere led to the search for an indirect mechanism of the influence of solar processes on the incoming radiation budget. Sources of solar influence include short-wave and UV radiation and corpuscular fluxes (GCRs, solar proton precipitation, high-energy particles). Their effects change the state of the ozone layer and the global electrical circuit, as well as strato-tropospheric circulation and cloud microphysics [Mironova et al., 2015; Krivolutsky et al., 2017; Harrison, Lockwood, 2020; Veretenenko et al., 2023a]. The physical model developed at ISTP SB RAS describes the electromagnetic interaction between the components of the magnetosphere—ionosphere—troposphere system. In contrast to the Tinsley model [Tinsley, 2008], in this model a change in the optical properties of water vapor in the IR range, namely, a change in the absorption of radiation by water dimers in the water vapor lines and continuum, results in an increase in the greenhouse effect, which causes dynamic changes in the troposphere. Since water vapor is unevenly distributed in space, an inhomogeneous tropospheric response is observed, in particular as formation or redistribution of clouds in height, which reduces the outgoing longwave radiation (OLR), thereby changing the radiation budget of the troposphere [Molodykh et al., 2020].

Let us take a closer look at the description of IR radiation absorption by water vapor. The infrared spectrum of water vapor absorption is known to consist of separate spectral lines and atmospheric windows located between them. In these windows, the absorption is weakly selective, or continuous, and the absorption spectrum is a water vapor continuum. Absorption by water dimers (complexes of two molecules) is the dominant factor in the absorption of self-continuum, i.e. water vapor absorption in a clear atmosphere.

Since the discovery of continuous absorption of radiation by water vapor, a large number of studies have been conducted, mainly in the atmospheric windows of near-IR and visible ranges. It has been experimentally established that the continuous absorption in the 8–12 μm atmospheric window is proportional to the square of the partial pressure of water vapor and decreases exponentially with increasing temperature [Ptashnik, 2015].

The features of the continuum make it possible to distinguish it spectrally against the background of a stronger intensity of water absorption lines, as a result the restoration of the continuum in atmospheric microwindows between water vapor absorption bands worked out. The mechanism based on the absorption of radiation by water dimers well explains the main temperature and spectral dependences of the water vapor continuum in the absorption bands. Properties of water dimers (dissociation energy and lifetime) allow them to be classified as stable (bound), or s-dimers, and meta-

stable (quasibound), or m-dimers, having different spectral characteristics. Absorption of stable or metastable dimers prevails in the continuum of water absorption, depending on thermodynamic conditions: s-dimers are common at lower temperatures; and m-dimers, at higher temperatures. The transition temperature in one direction or another depends on the intermolecular potential and varies for different molecular pairs, for example, for water dimers it is close to room temperature. Accordingly, the proportion of stable and metastable dimers in water vapor is approximately the same for atmospheric conditions. Model calculations have shown that the semi-empirical model of water dimer absorption better reproduces the experimental in-band self-continuum in the near IR range. Due to its spectral length (the atmospheric window in the mid-IR range and the contribution of spectral sections of water absorption lines), continuous absorption of water vapor can lead to a decrease in OLR, thereby affecting the radiation budget of the climate system [Simonova et al., 2022]. Based on the above ideas, in this paper we analyze the relationship of variations in the electric potential (EP) of the ionosphere with meteorological parameters (OLR, radiation absorption by water vapor in the 8–12 μm atmospheric window, upper cloudiness) for disturbed conditions in interplanetary space.

DATA AND ANALYSIS METHOD

The observed climatic changes, especially at high latitudes, require a more detailed study of the influence of physical processes occurring in near-Earth space on the lower atmosphere. This is necessary to parameterize them in order to include them in numerical climate models. We have previously used the *PC* geomagnetic activity index, which describes geomagnetic disturbances in the polar cap [Troshichev et al., 1988; https://pcindex.org /], as a solar activity proxy to study solar-tropospheric relations. This geomagnetic index reflects the expected physical processes, yet their parameterization results in the following disadvantages: 1) the integral characteristic of solar activity at the boundary of the magnetosphere; 2) the need to include a model of the magnetosphere; 3) the integral characteristic of solar activity in the ionosphere. These disadvantages complicate the use of the *PC* index due to the irregularity in the tropospheric response to solar influence. In this regard, we have taken EP as the optimal characteristic of solar influence on the troposphere. This heliogeophysical parameter describes the expected physical processes, and applying the Weimer model to its calculation allows us to parameterize processes in the magnetosphere and to obtain a spatial distribution of EP in the ionosphere.

A few words about the Weimer model, which we use to calculate EP. We have employed the 2001 version in our research before; in this work, calculations are performed with the latest version of the model, i.e. the 2005 version [Weimer, 2001, 2005]. Let us focus on the main modifications made to the model to improve it:

1. More accurate field values and more precise location of the low-latitude boundary of the convection electric field.

2. Spherical harmonic functions are used only within a small region at the pole. At lower latitudes, potentials are constructed from several functions of the Fourier series of longitude with discrete latitude steps, i.e. the calculation is made in a circle with a radius that varies depending on interplanetary magnetic field (IMF) and solar wind parameters with a constant shift of 4.2 °.

3. Nonlinear effects of saturation of the relationship between the solar wind and the magnetosphere are better reproduced for normal IMF conditions, but it is necessary to control the results of applying the model to cases with strong IMF.

Figure 1 illustrates the spatial distribution of EP calculated for the events on November 20, 2003 (left) and July 15, 2000 (right). As a quiet period, we have taken 2009. The top panel presents calculations with the 2001 model; the bottom panel, with the 2005 model.

The spatial distribution of EP for the quiet period according to the 2005 model differs from that obtained by the 2001 model by a slight increase in positive and negative potentials. Significant differences in the EP structure are observed during disturbance maximum: in the 2005 model, there is an increase in both the region and the magnitude of the negative potential, whereas in the 2001 model, the positive potential increases more considerably. The detected differences are related to the shift in the convection zone to the nightside due to improvements made to the 2005 model.

For further analysis, the spatial contrast of EP was utilized as a characteristic of solar influence. This parameter was obtained as follows. In the first step, the 2005 Weimer model [https://zenodo.org/records/2530324] was employed to calculate the spatial distribution of EP anomalies whose structure consists of two regions (of negative and positive sign). The EP anomalies were calculated from the formula

$$EP_i = EP_i - \langle EP \rangle, \quad (1)$$

where i is the hour number; $<EP>$ is the average over seven preceding days.

In the second step, the spatial distribution of the EP contrast was constructed according to the formula

$$\Delta EP_i = \langle EP_i^+ \rangle - \langle EP_i^- \rangle, \quad (2)$$

where i is the hour number; $<EP_i>$ is the average over the region of one sign.

Changes in the EP anomalies and contrast averaged over latitudes above 60° N were analyzed using the November 20, 2003 and April 23, 2023 events (see Table), triggered by a classical coronal mass ejection, as an example. The selected magnetic superstorms are similar in conditions of development of interplanetary disturbances, which caused the storms [Grechnev et al., 2014; Abunina et al., 2024]. The choice of the magnetic storms in different seasons also allowed us to additionally take into account seasonal variations of geomagnetic activity with a maximum in spring and autumn, which can manifest themselves in variations of meteorological parameters during disturbances [Karakhanyan, Molodykh, 2025].

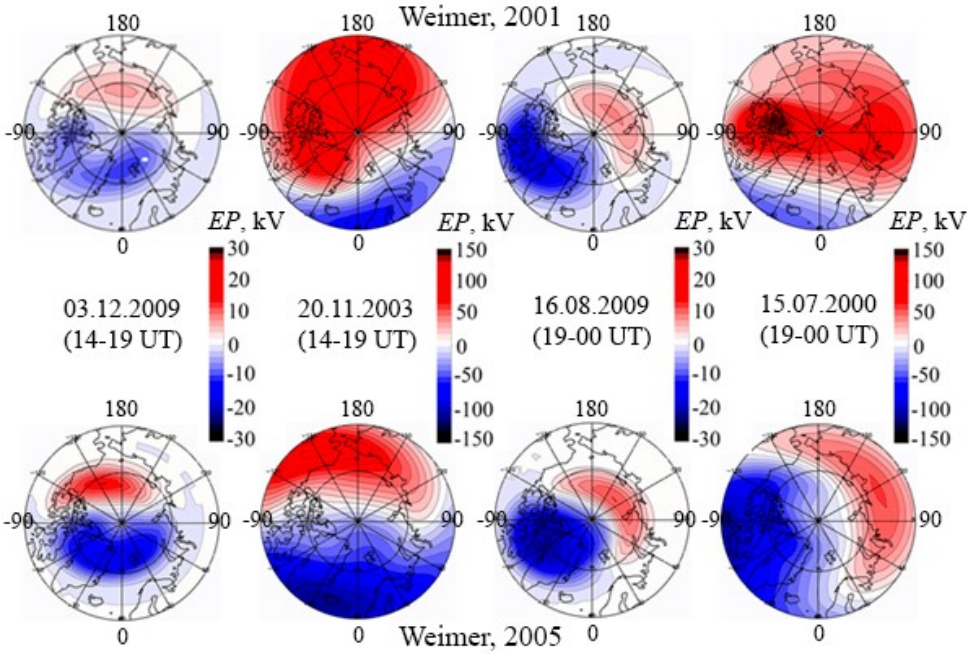

Figure 1. Spatial distributions of EP calculated using two Weimer model versions for quiet conditions in 2009 and powerful geomagnetic storms on November 20, 2003 and July 15, 2000

Interplanetary medium parameters during magnetic superstorms

Event date	V_{max}, km/s	n, cm^{-3}	$B_{z_{max}}$, nT	B_y, nT	AL, nT	Date and value of Dst, nT
Nov. 20–21, 2003	703	7.6	–50.9	22.5	–1790	Nov. 20, 2003, Dst=–422 nT
Apr. 23–24, 2023	711*	10.2*	–32.4*	–2.5*	–1015*	Apr. 24, 2023, Dst=–213* nT

*Preliminary data [https://omniweb.gsfc.nasa.gov/html/ow_data.html; https://wdc.kugi .kyoto-u.ac.jp/wdc/Sec3.html]

Ionospheric EP was calculated by the Weimer model from hourly data on the solar wind and IMF parameters obtained from the OMNI database [https://omniweb.gsfc.nasa.gov/html/ow_data.html].

The method of calculating the EP contrast was also employed to compute the contrast of meteorological parameters in order to conduct a comparative analysis of EP with meteorological parameters during disturbances. We used hourly meteorological values in a 1.0°×1.0° grid from the dataset [Wielicki et al., 1996; https://ceres-tool.larc.nasa.gov/ord-tool/jsp/SYN1degEd41Selection.jsp/]. Note that in the troposphere there is a natural synoptic period (NSP) — a period during which cyclones/anticyclones continue to move and the location of their centers in a certain region of Earth or in the entire hemisphere (NSP ~7 days) remains unchanged. To minimize the influence of synoptic processes, weather parameter anomalies were calculated relative to the average over seven days before the event. OLR is represented by the broadband heat flux observed by CERES at the upper boundary of the troposphere (h~20 km); radiation absorption by water vapor in the 8–12 μm atmospheric window, by the radiated heat flux (h~20 km) of the CERES infrared atmospheric window (8–12 μm). The upper cloudiness is characterized by the number of high-level clouds (from 300 hPa to the tropopause) as a percentage of sky cover.

RESULTS

Spatial distributions of EP during disturbances (see Figure 1), obtained by the 2001 and 2005 versions of the Weimer model, differ significantly.

Let us analyze the dynamics of EP variations averaged over latitudes above 60° N during November 20, 2003 and April 23, 2023 geomagnetic superstorms. Figure 2 illustrates variations in EP anomalies (top panels) and EP contrast (bottom panels), calculated by the two Weimer model versions. Comparative analysis has shown that during the magnetic superstorms the contribution of negative EP values to the overall variability in EP anomalies is greater in the 2005 model than in the 2001 model. This difference is related to the above modifications made to the 2005 model. Variations in EP contrast during disturbances, calculated by the 2001 model, correlate well with those obtained by the 2005 model. The EP contrast behavior in the two Weimer model versions agrees better than the dynamics of EP anomalies for the high-latitude region.

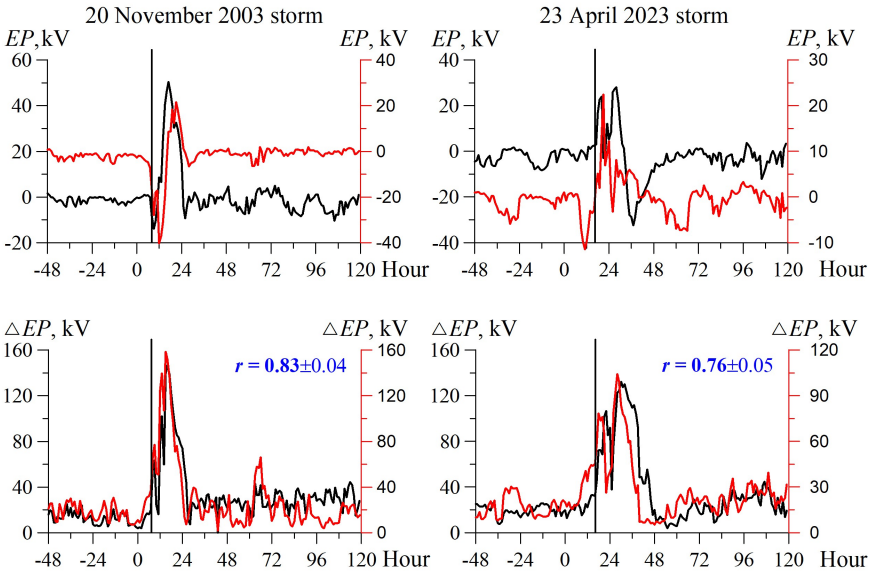

Figure 2. Variations in EP anomalies (top) and EP contrast (bottom), averaged over latitudes above 60° N, during magnetic superstorms: the 2001 Weimer model (black line), the 2005 Weimer model (red line); onset of the geomagnetic storm (vertical line); zero on the X-axis is 00 UT of the day when the geomagnetic storm began

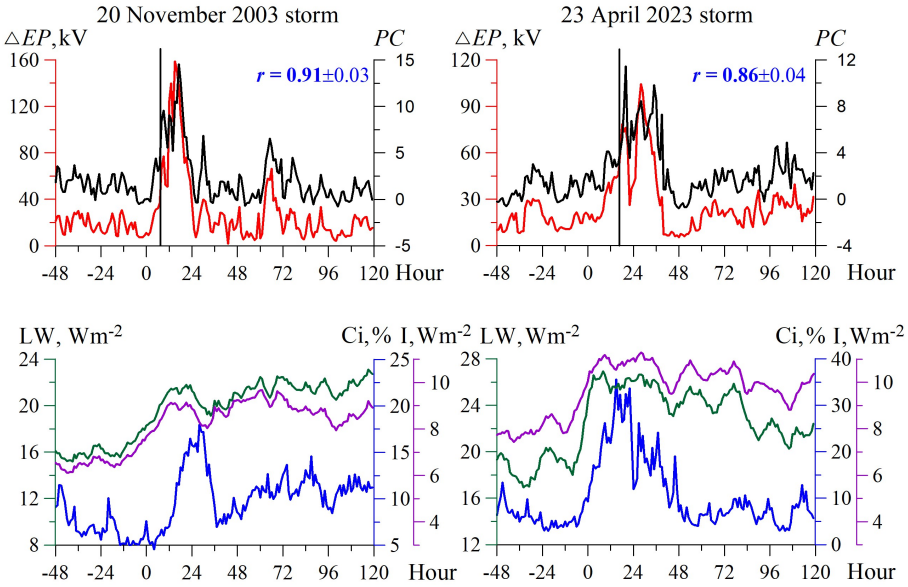

Figure 3. Variations in EP contrast (top panels, red line) and contrast of meteorological parameters (bottom panels) averaged over latitudes above 60° N: OLR (green line); radiation absorption by water vapor in the 8–12 μm atmospheric window (*I*, purple line); upper cloudiness (*Ci*, blue line), as well as variations in the *PC* geomagnetic index (top panels, black line) during magnetic superstorms. The vertical line indicates the onset of the geomagnetic storm; zero on the X-axis is 00 UT of the day when the geomagnetic storm began

Let us examine the linear relationship of variations in the EP contrast, averaged over latitudes above 60° N, with variations in the *PC* geomagnetic index during the November 20, 2003 and April 23, 2023 magnetic superstorms. The correlation is 0.71±0.5 between variations in the EP contrast, calculated by the 2001 Weimer model, and variations in the *PC* index for the cases considered.

The EP contrast variations calculated by the 2005 model correlate better with the *PC* index variations for the geomagnetic storms under study (Figure 3, top panels). The high correlation coefficient between the parameters allows us to say that the *PC* index can be used as an indicator of solar activity during isolated magnetic superstorms.

To determine the tropospheric response to changes in the potential during the magnetic storms, we use the EP contrast calculated by the 2005 Weimer model (see Figure 3, at the top). During the November 20, 2003 magnetic superstorm, an increase in the EP contrast was accompanied by an increase in the contrast of meteorological parameters, especially in the contrast of upper cloudiness. The maximum contrast of meteorological

parameters was observed within the first 12 hrs relative to the maximum contrast of EP. For the April 23, 2023 geomagnetic storm, the noted features in the change in the parameters considered are less pronounced, possibly due to the influence of substorm activity observed before the onset of the magnetic storm and resulting from amplification of field-aligned currents caused by the electric field of magnetospheric convection, which occurs when the solar wind and IMF interact with the magnetosphere.

Variations in upper cloudiness anomalies have a unidirectional trend with the dynamics of EP anomalies at high latitudes during geomagnetic superstorms (Figure 4). The features characteristic of the dynamics of the contrast of the parameters under study persist in the behavior of their anomalies. However, the amplitude of the response of positive upper cloudiness anomalies to a change in positive EP is by an order of magnitude higher than the amplitude of the response of negative upper cloudiness anomalies to a change in negative EP. Look at the maps of EP anomalies and the spatial distribution of upper cloudiness anomalies (Figure 5) during the April 23, 2023 magnetic storm. Under quiet conditions at latitudes above 60° N, upper cloudiness anomalies are uniformly distributed and amount to few percent. The greatest increase in upper cloudiness is observed in the region of increased positive potential, which has a nonlinear effect on properties of water vapor, in this case coming from midlatitudes with cyclones that occur near the eastern coast of Eurasia and, moving to the northeast, reach their maximum near the Aleutian Islands.

DISCUSSION

Our planet as an open system is affected by changes in the solar wind due to active processes on the Sun. Rapid climate changes on Earth sustain the discussion about the magnitude and nature of solar influence on the lower atmosphere. The spatial inhomogeneity of the tropospheric response to solar influence may show up to a greater extent in the regional climate variability due to changes in the optical properties of water vapor in the troposphere during geomagnetic disturbances [Karakhanyan, Molodykh, 2025]. Local climate changes (high latitudes, inland regions) under the influence of solar processes can be examined in detail on the basis of data obtained from the ISTP SB RAS instrumentation, in particular from the Unique Research Facility "Optical Instruments" [https://iszf.irk.ru/usu-optical-instruments/].

In our study, we have used the contrast in EP variations, which is a proxy of solar activity. This enabled us to minimize the differences between its calculations for different Weimer model versions (see Figure 2). A high correlation is shown between variations in the EP contrast averaged over the high-latitude region and variations in the *PC* geomagnetic index (see Figure 3). This finding allows us to recommend both characteristics as an indicator of solar activity when studying magnetic superstorms. The spectrum of meteorological parameters consists of high-frequency (daily, seasonal, annual, and 2–5-year variations) and low-frequency components. The latter contains variations close to heliogeophysical periods, in particular a ~22-year variation similar to the Hale magnetic cycle on the Sun was found in the variability in trajectories of extratropical cyclones in the North Atlantic [Veretenenko et al., 2023b]. Since the solar signal present in the meteorological parameters has an amplitude lower than the amplitude of their daily and seasonal variations, we study variations not in the value itself, but in the anomalies or deviations of the meteorological parameters from their mean during disturbance. By the example of geomagnetic superstorms of

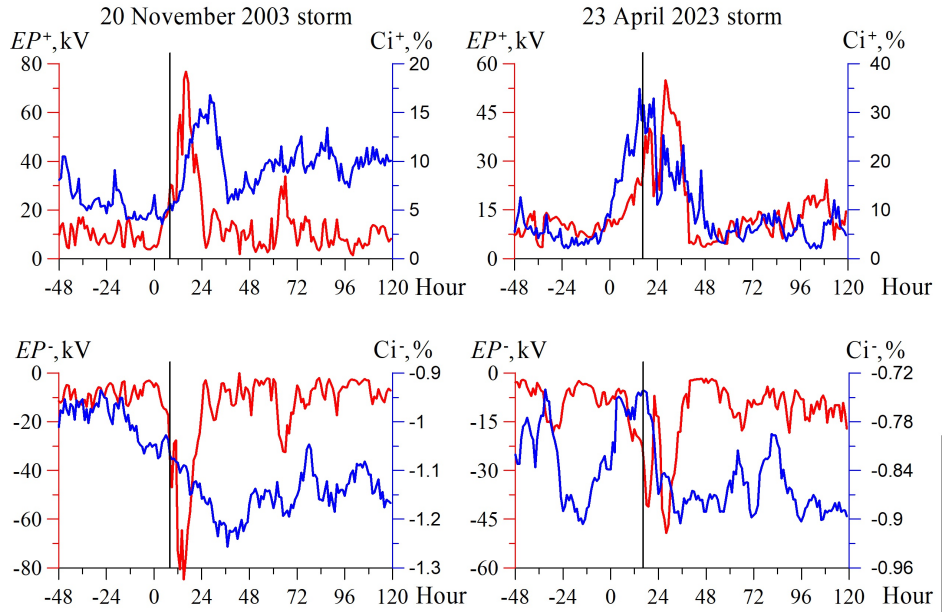

Figure 4. Variations in positive (top) and negative (bottom) EP anomalies (red curves) and upper cloudiness anomalies (blue curves), averaged over latitudes above 60° N, during magnetic superstorms. The vertical line indicates the onset of the geomagnetic storm; zero on the X-axis is 00 UT of the day when the geomagnetic storm began

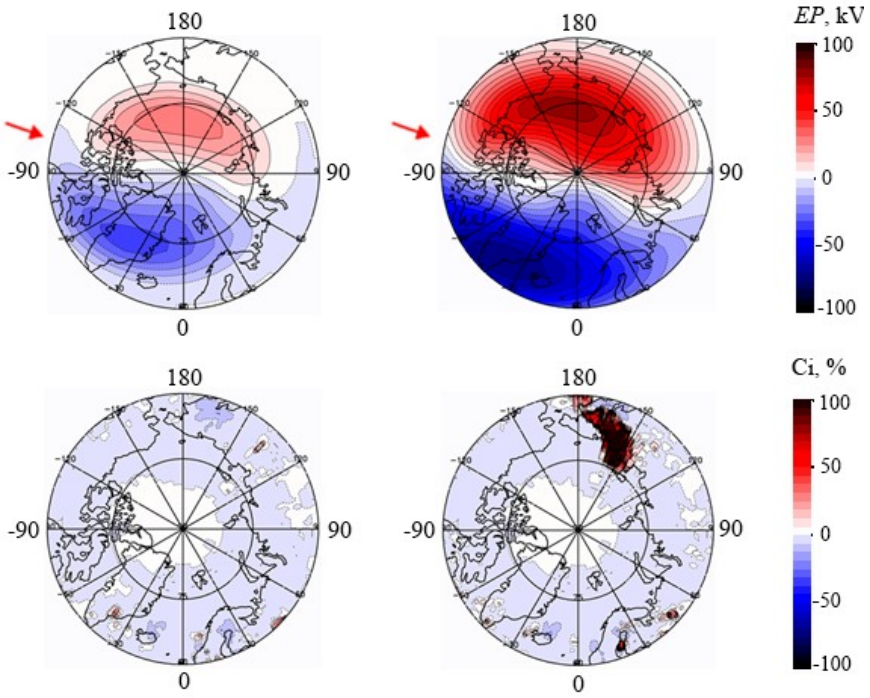

Figure 5. Spatial distributions of EP anomalies (top) and upper cloudiness (bottom) during the quiet period (left) and during their maximum (right) for an average of 3 hrs from 18 UT to 20 UT for latitudes above 60° N during the April 23, 2023 geomagnetic superstorm. The midday meridian is indicated by arrows

solar cycles 23 and 25, which are moderate and the second components of the 22-year magnetic activity cycle [Ishkov, 2010, 2024], we have shown that during individual severe disturbances an increase in the EP contrast is accompanied by an increase in the contrast of meteorological parameters, especially in the contrast of upper cloudiness (see Figure 3). For meteorological parameters, the contrast was utilized as an integral characteristic to illustrate the amplitude of variations in the meteorological response to solar influence due to the inhomogeneous structure of the tropospheric response in space. The results of the study have been obtained using the model of the mechanism of indirect influence of solar processes on the radiation budget of the climate system, developed at ISTP SB RAS. They will help to parameterize physical processes in the troposphere in accordance with the proposed scenario and hence to include solar activity, along with the solar constant, in climate models.

CONCLUSIONS

Analysis of the relationship of EP variations with variations in meteorological parameters during magnetic superstorms allowed us to obtain the following results.

Spatial distributions of EP obtained using the 2001 and 2005 Weimer model versions differ most considerably during the maximum of the disturbance.

Variations in EP anomalies averaged over latitudes above 60° N differ significantly in the Weimer model versions considered. However, variations in the average EP contrast calculated by the 2001 and 2005 versions occur synchronously during severe disturbances.

Correlation analysis of variations in the average EP contrast with variations in the *PC* geomagnetic index has shown that both characteristics can be used as a proxy of solar activity to study isolated severe disturbances.

During the disturbances, an increase in the EP contrast is accompanied by an increase in the contrast of meteorological parameters, especially in the contrast of upper cloudiness.

The work was financially supported by the Ministry of Science and Higher Education of the Russian Federation.

REFERENCES

Abunina M.A., Shlyk N.S., Belov S.M., et al. On the most interesting events in the solar wind and cosmic rays in 2023–2024. *Mezhdunarodnaya Baikal'skaya molodezhnaya nauchnaya shkola po fundamental'noi fizike. Trudy XVIII Konferentsii molodykh uchenykh «Vzaimodeistvie polei i izlucheniya s veshchestvom»* [The Baikal Young Scientists' International School on Fundamental Physics. Proc. XVIII Young Scientists' Conference "Interaction of Fields and Radiation with Matter"]. Irkutsk, 2024, pp. 5–7. (In Russian).

Grechnev V.V., Uralov A.M., Chertok I.M., et al. A challenging solar eruptive event of 18 November 2003 and the causes of the 20 November geomagnetic superstorm. IV. Unusual magnetic cloud and overall scenario. *Solar Phys.* 2014, vol. 289, iss. 12, pp. 4653–4673. DOI: 10.1007/s11207-014-0596-5.

Harrison R.G., Lockwood M. Rapid indirect solar responses observed in the lower atmosphere. *Proc. Roy. Soc. A.* 2020, vol. 476, iss. 2241, 20200164. DOI: 10.1098/rspa.2020.0164.

Ishkov V.N. Properties and surprises of solar activity XXIII cycle. *Sun and Geosphere*. 2010, vol. 5, iss. 2, pp. 43–46.

Ishkov V.N. Current solar cycle 25 on the eve of the maximum phase. *Geomagnetism and Aeronomy*. 2024, vol. 64, iss. 7, pp. 1167–1175. DOI: 10.1134/S0016793224700257.

Karakhanyan A.A., Molodykh S.I. A decline of linear relation between outgoing longwave radiation and temperature during geomagnetic disturbances. *JASTP*. 2025, vol. 270, iss. 5, 106503. DOI: 10.1016/j.jastp.2025.106503.

Krivolutsky A.A., Vyushkova T.Y., Mironova I.A. Changes in the chemical composition of the atmosphere in the polar regions of the Earth after solar proton flares (3D modeling). *Geomagnetism and Aeronomy*. 2017, vol. 57, iss. 2, pp. 156–176. DOI: 10.1134/ S0016793217020074.

Mironova I.A., Aplin K.L., Arnold F., et al. Energetic particle influence on the Earth's atmosphere. *Space Sci. Rev.* 2015, vol. 194, iss. 1-4, pp. 1–96. DOI: 10.1007/s11214-015-0185-4.

Mokhov I.I. Russian climate research in 2019–2022. *Izvestiya RAN. Fizika atmosfery i okeana* [Izvestiya, Atmospheric and Oceanic Physics]. 2023, vol. 59, iss. 7, pp. 830–851. (In Russian).

Molodykh S.I., Zherebtsov G.A., Karakhanyan A.A. Estimation of solar activity impact on the outgoing infrared-radiation flux. *Geomagnetism and Aeronomy*. 2020, vol. 60, iss. 2, pp. 205–211. DOI: 10.1134/ S0016793220020103.

Ptashnik I.V. Water vapour continuum absorption: short prehistory and current status. *Optika atmosfery i okeana* [Atmospheric and Oceanic Optics]. 2015, vol. 28, iss. 5, pp. 443–459. (In Russian).

Simonova A.A., Ptashnik I.V., Elsey J., et al. Water vapour self-continuum in near-visible IR absorption bands: Measurements and semiempirical model of water dimer absorption. *J. Quantitative Spectroscopy and Radiative Transfer*. 2022, vol. 277, iss. 1, 107957. DOI: 10.1016/j.jqsrt.2021.107957.

Tinsley B.A. The global atmospheric electric circuit and its effects on cloud microphysics. *Rep. on Progress in Physics.* 2008, vol. 71, iss. 6, 066801. DOI: 10.1088/0034-4885/71/6/066801.

Troshichev O.A., Andrezen V.G., Vennerstrom S., Friis-Christensen E. Magnetic activity in the polar cap – A new index. *Planet. Space Sci.* 1988, vol. 36, iss. 11, pp. 1095–1102. DOI: 10.1016/0032-0633(88)90063-3.

Veretenenko S.V., Dmitriev P.B., Dergachev V.A. Long-term effects of solar activity on cyclone tracks in the North Atlantic. *St. Petersburg State Polytechnical University J.: Physics and Mathematics*. 2023a, vol. 16, iss. 1.2, pp. 454–460. DOI: 10.18721/JPM.161.269.

Veretenenko S.V., Dmitriev P.B., Dergachev V.A. Long-term changes main trajectories of extratropical cyclones in the North Atlantic and their possible association with solar activity. *Geomagnetism and Aeronomy*. 2023b, vol. 63, iss. 7, pp. 953–965. DOI: 10.1134/s0016793223070265.

Weimer D.R. An improved model of ionospheric electric potentials including substorm perturbations and application to the Geospace Environment Modeling November 24, 1996, event. *J. Geophys. Res.: Space Phys.* 2001, vol. 106, iss. A1, pp. 407–416. DOI: 10.1029/2000JA000604.

Weimer D.R. Improved ionospheric electrodynamic models and application to calculating Joule heating rates. *J. Geophys. Res.* 2005, vol. 110, iss. A5, A05306. DOI: 10.1029/2004 JA010884.

Wielicki B.A., Barkstrom B.R., Harrison E.F., et al. Clouds and the Earth's Radiant Energy System (CERES): An Earth observing system experiment. *Bull. American Meteorological Society.* 1996, vol. 77, iss. 5, pp. 853–868. DOI: 10.1175/1520-0477(1996)077<0853:CATERE>2.0.CO;2.

URL: https://zenodo.org/records/2530324 (accessed April 4, 2025).

URL: https://omniweb.gsfc.nasa.gov/html/ow_data.html (accessed April 4, 2025).

URL: https://iszf.irk.ru/usu-optical-instruments/ (accessed April 4, 2025).

URL: https://ceres-tool.larc.nasa.gov/ord-tool/jsp/SYN1degEd41Selection.jsp (accessed April 4, 2025).

URL: https://www.ipcc.ch/report/ar6/syr/ (accessed April 4, 2025).

URL: https://wdc.kugi.kyoto-u.ac.jp/wdc/Sec3.html (accessed April 4, 2025).

URL: https://pcindex.org/ (accessed April 4, 2025).

The paper is based on material presented at the 20th Annual Conference on Plasma Physics in the Solar System, February 10–14, 2025, Space Research Institute of the Russian Academy of Sciences, Moscow, Russia.

Original Russian version: Karakhanyan A.A., Molodykh S.I., published in Solnechno-zemnaya fizika. 2025, vol. 11, no. 3, pp. 100–107. DOI: 10.12737/szf-113202511.

How to cite this article

Karakhanyan A.A., Molodykh S.I. Meteorological response to changes in ionospheric electric potential caused by disturbed solar wind. *Sol.-Terr. Phys*. 2025, vol. 11, iss. 3, pp. 91–97. DOI: 10.12737/stp-113202511.